Sulfonated graphenes: Efficient solid acid catalyst for the 1 glycerol valorization 2 3

Ludovic Pinard, Cristian Miranda, Alfonso Ramírez, Alexander Sachse, Yannick Pouilloux, Julian Urresta, Ludovid Pinard

Sulfonated graphenes: Efficient solid acid catalyst for the glycerol valorization

Cristian Miranda[ab*], Alfonso Ramírez[c], Alexander Sachse[b], Yannick Pouilloux[b], Julian Urresta[a*], Ludovid Pinard[b].

[a] *Laboratorio de Investigación en Catálisis y Procesos (LICAP) – Universidad del Valle, Ciudad Universitaria Meléndez, Calle 13 # 100-00, Cali - Colombia.*

[b] *Institut de Chimie des Milieux et Matériaux de Poitiers (ICM2P), UMR 7285 CNRS, 4 Rue Michel Brunet, Bâtiment B27, 86073, Poitiers Cedex – France.*

[c] *Grupo Catálisis, Departamento de Química, Universidad del Cauca, Carrera 3 No. 3N-100, Popayán-Colombia.*

*** Corresponding author:** julian.urresta@correounivalle.edu.co (Julian Urresta) miranda.cristian@correounivalle.edu.co (Cristian Miranda)

Abstract

Heterogeneous acid catalysts were obtained based on the functionalization of reduced graphene oxide. The synthesis involves i) the obtaining of graphene oxide by the modified Hummers method ii) the reduction of graphene oxide by three different routes, through the use of hydrazine dihydrochloride, Zn/HCl and ascorbic acid, and iii) the grafting of sulfonic groups in the surface of graphene oxides with 4-diazonium benzenesulfonate. These solids were characterized and evaluated in the etherification of glycerol with *tert*-butyl alcohol, finding in general glycerol conversions higher than those obtained with a sulfonic resin (Amberlyst® 15). In addition, the selectivity depends on the reduction route used to obtain the catalyst; A larger amount of oxygen groups remaining after the reduction, helps the formation of *poly*-substituted ethers. These solids also showed stability in their use, converting them into highly efficient catalysts in the valorization of glycerol.

Key words: Reduced sulfonated graphene oxide, ascorbic acid reduction, glycerol etherification, *tert*-butyl alcohol, glycerol ethers.

1. Introduction

The large production of biodiesel has increased the production of glycerol, which is a byproduct of this process. According to estimates, glycerol production will be six times higher than global demand within a few years from now [1,2]. The glycerol conversion into value-added products is thus an alternative for glycerol disposal and its surplus problem. One promising way to valorize this polyol is through its conversion into glycerol ethers, which can then be used as oxygenated fuel additive, intermediates in the pharmaceutical industry and non-ionic surfactants [3-5]. The etherification of glycerol with isobutene or *tert*-butyl alcohol allows obtaining different ethers depending on the degree of substitution. For applications of these ethers as oxygenated additives, *poly*-substituted ethers (*di* and *tri*-ethers) are preferred due to their physical-chemical properties that are compatible with fuel formulations, while the mono-ether is not suitable for this use due to its low solubility in diesel [6].

The synthesis of glycerol *tert*-butyl ethers using isobutene has been extensively investigated [7-10]. Yet it requires high pressures to ensure contact with glycerol. Additionally, isobutene is separated as a vapor stream at the outlet of the reactor and must be recompressed before recycling, which is another drawback of the process [11]. The use of *tert*-butyl alcohol as an etherifying agent has been less studied. The etherification between glycerol and *tert*-butyl alcohol can be catalyzed by acids. When this type of catalysis and *tert*-butyl alcohol is used as an etherifying agent, water is obtained as a by-product, which implies that the selected catalyst must be active in the presence of water and, at the same time, the presence of this by-product can alter the equilibrium of the formation of the glycerol *poly*-substituted ethers [12].

The use of homogeneous catalyst such as strong acid (e.g. H_2SO_4) [13] causes corrosion and environmental issues. These can be overcome by using solid acid catalysts such as acid ion-exchange resin, but these have a poor thermal stability [14]. Zeolites are a family of microporous minerals that feature important Brønsted acidy and high thermal stability [14,15]. The use of zeolites in the glycerol etherification has recently allowed to deduce that shape selective and confinement properties can drive activity, selectivity and stability of the catalytic process [16].

Carbon materials are attractive metal-free, stable, cheap, and recyclable catalysts that allow in any cases to achieve green and sustainable catalytic transformations [17]. Solid acid catalysts prepared from functionalized carbons were used in the etherification of glycerol by *tert*-butyl alcohol. Janaun and Ellis [18] obtained a sulfonated carbon catalyst from sugar that showed important activity featuring high thermal resistance. Moreover, Galhardo *et al*. [19] report on obtaining sulfonated carbon from agro-industrial waste and its subsequent use as acid catalyst in the glycerol etherification with *tert*-butyl alcohol. Highest conversions were achieved (53%) at 393 K using a *tert*-butyl alcohol: glycerol molar ratio of 4 and 5% of catalyst. In this case the selectivity towards *di*- and *tri*-substituded ethers was 25% after 4 h of reaction. Frusteri *et al.* [7] obtained mono-disperse carbon microspheres via a hydrothermal carbonization process, which were functionalized with acid groups and used in the etherification of glycerol with *tert*-butyl alcohol. In spite of having a lower acidity than Amberlyst® 15, these showed high activity in terms of glycerol conversion and also, they were also stable by retaining the functionalized groups after their use.

Among carbons, graphene oxide (GO) and related materials are an emerging new type of very promising carbocatalysts due to their unique properties, including 2D structure,

high stability, and high flexibility for the introduction of catalytic functions [17]. Recently, several authors reported that sulfonated graphene demonstrated excellent activities and selectivities in different acid-catalyzed reactions, including reactions that involve water formation [20-23]. Zhou *et al.* [24] reported the synthesis of sulfonated graphene by its functionalization through sulfonic acid grafting and its application in the glycerol etherification with isobutene at 333–343 K employing 4 wt% catalyst and a molar isobutene/glycerol ratio of 4. Complete glycerol conversion was achieved within 7 h with high selectivity (92 mol%) toward the desired *poly*-substituted ethers.

Although this material has been used as an acid catalyst, its particular activity, even in the presence of water, makes it a good candidate to be evaluated in the etherification of glycerol with *tert*-butyl alcohol. In the present study, we compare three synthesis procedures for the development of sulfonated reduced graphene oxide. We compare the impact the new catalysts to usually employed sulfonated resins and sufonated active carbon on activity, selectivity and stability of the etherification process.

2. Experimental section

2.1. Chemicals and catalysts

Glycerol (99%) and *tert*-butyl alcohol (99.4%) were obtained from Fisher and Merck respectively. Commercial activated carbon (G60) was obtained from Darco. Amberlyst® 15 (dry) ion-exchange resin was purchased from Across Organic. Graphite powder (<20 μm, synthetic) was obtained from Sigma-Aldrich. The preparation of catalysts based on graphene oxide is described below.

Preparation of graphene oxide

Graphene oxide was synthesized from graphite powder by a modified Hummers method as originally presented by Kovtyukhova, *et al.* [25,26]. For this purpose, 2.01 g of graphite powder was mixed with 5.00 mL of concentrated sulfuric acid, 2.12 g of potassium persulfate and 2.06 g of phosphorus pentoxide. This mixture was heated to 353 K for 2 h. The solid was then filtered using a 0.2 micron Millipore nylon filter and washed first with 100 mL of deionized water, then with 200 mL of methanol and finally with 200 mL of ethyl acetate (what we will call washes W-M-EA). The resulting pretreated graphite (PG) was dried at 313 K for 12 h. Then, 2.16 g of PG was mixed with 55 mL of sulfuric acid at 273 K and 7.47 g of potassium permanganate was then added portionwise. The reaction mixture was stirred at 308 K for 2 h and then cooled to 273 K, followed by the addition of an aqueous solution of 7.5% (v/v) hydrogen peroxide. The solid was centrifuged to 4000 rpm during 30 min and the surnatant removed. The resulting solid was washed with W-M-EA and then was dried at 313 K for 12 h. This solid was named GO. **Figure S1**, shows the synthesis scheme.

Reduction of graphene oxide

The reduction of graphene oxide was carried out by three different routes: with i) hydrazine dihydrochloride, ii) ascorbic acid [27] and iii) Zn/HCl [28]. For the first route, 1.02 g of GO was sonicated in 500 mL of deionized water for 2 h. Subsequently, 3.02 g of Na_2CO_3 was added to reach a pH of 9. Then, 30.04 g of hydrazine dihydrochloride was added to the suspension and the mixture was refluxed for 24 h. The solution was cooled down to room temperature (293 K) and filtered through a nylon filter (0.45 mm, 47 mm) and the solid was washed with W-M-EA. The powder was dried at 333 K for 12 h. The solid obtained by this route was named (GO)R_H. For the reduction with ascorbic acid, 0.512 g of GO was sonicated in 600 mL of deionized water for 2 h. Then, 164.10 g of ascorbic acid was added

at 353 K under stirring for 2 h. The solution was cooled down to room temperature (293 K) and filtered through a nylon filter and washed with W-M-EA. The powder was dried at 333 K for 12 h. The solid obtained was named (GO)R_A. Finally, for the reduction with Zn/HCl, 0.503 g of GO was sonicated in 500 mL of deionized water for 2 h and acidified (pH=1.9) with concentrated HCl. Then, 1.00 g of zinc powder was added at room temperature (298 K) under stirring for 10 min, follow by the addition of 125 mL of concentrated HCl. After 1 h, the solid was filtered through a nylon filter and washed with 1.5 L of deionized water. The black powder was dried at 333 K for 12 h. The obtained solid was named (GO)R_Z. **Figure S2**, shows the synthesis scheme.

Sulfonation of reduced graphene oxide

Graphene oxide (GO) as well the reduced graphene oxides (GO)R_H, (GO)R_A, and (GO)R_Z, were sulfonated through treatment with 4-benzenediazoniumsulfonate which was *in situ* generated. For this purpose, 0.273 g of the initial solid was sonicated in 40 mL of deionized water for 2 h. Then, 0.947 g of sodium nitrite and 0.795 g of sulfanilic acid were added to the resulting solution, allowing the *in situ* formation of the diazonium salt, and the reaction was conducted at 298 K for 24 h. The solution was filtered through a nylon filter and washed with 150 mL of 1M HCl and 250 mL of acetone. The powder obtained was dried at 313 K at 333 K for 12 h. The resulting samples were named (GO)-S, (GO)R_H-S, (GO)R_A-S, and (GO)R_Z-S. **Figure S3**, shows the synthesis scheme.

In order of comparison, activated carbon (G60) was similarly sulfonated to graphene oxide (AC)-S, reduced with hydrazine dihydrochloride (AC)R_H and, finally, the reduced solid was sulfonated to obtain (AC)R_H-S.

2.2. Characterization of catalysts

Textural properties

Surface area measurements were conducted through applying the BET equation to nitrogen physisorption isotherms at 77 K measured in a TriStar II plus. The samples were outgassed at 3 mTorr and 423 K for 12 h prior to analysis. Characterization by transmission electron microscopy (TEM) was carried on a JEOL JEM-2011TEM. To prepare samples for TEM, graphene derived samples were dispersed in ethanol, and deposited onto copper grids. Scanning electron microscopy (SEM) images were obtained on a JEOL JSM-790CF microscope. X-ray powder diffraction (XRD) patterns were recorded at room temperature on Empyrean X-ray diffractometer (Malvern Panalytical Ltd., Royston, UK) operating with Cu Kα radiation (λ = 0.15418 nm) with a scan speed of 1° min^{-1} and a scan range of 5–65° at 30 kV and 15mA. Raman spectroscopy was performed using a Raman HORIBA JOBIN YVON Labram HR800UV confocal microscope equipped with a Peltier cooled CCD detector. The exciter wavelength is 532 nm. The laser power delivered to the sample was 0.02 mW (use of an optical density filter). The device was equipped with an Olympus confocal microscope that allows working backscatter. A diffraction grating with 600 $lines.mm^{-1}$ was used and the opening of the confocal hole is 200 μm. The spectral resolution was 1.5 cm^{-1}. The spectrometer was calibrated with a silicon sample. The LabSpec 5 software allows the acquisition and processing of results.

Chemical composition

The contents of carbon, hydrogen, oxygen and sulfur in graphene-based catalysts were obtained with an elemental analyzer NA2100 Protein, Thermoquest Instruments.-XPS was performed in a high vacuum chamber (pressure ≤ 9×10^{-8} Pa) on a Kratos Axis Ultra DLD spectrometer equipped with a monochromatic radiation source Al Mono ($Al_{k\alpha}$: 1486.6 eV)

188 operating at 150 W (15 kV and 10 mA). Survey spectra were recorded with a step of 1 eV
189 (transition energy: 160 eV). Based on the collected basic information, high-resolution XPS
190 spectra were collected at a step of 0.1 eV (transition energy: 20 eV).
191
192 **Acid properties**
193 The acidity of GO samples and activated carbon was confirmed by Boehm titration. 0.1 g
194 of catalyst was added to 20 mL of 2 M NaCl solution. After 24 h of stirring at room
195 temperature, the solution was titrated with 0.1 M NaOH solution. The number of acid sites
196 was then calculated from the amount of NaOH required in the titration. This method has
197 been commonly used in previous studies, correlating the loading of SO_3H calculated by
198 elemental analysis [29-31]. For the Amberlyst® 15, Fourier transform Infrared spectra (FT-
199 IR) of pyridine adsorbed was used on a Nicolet Magna 550-FT-IR spectrometer with a 2
200 cm^{-1} optical resolution. The sample were first pressed into self-supporting wafers (diameter:
201 1.6 cm) and pretreated from room temperature to 403 K in an IR cell connected to a
202 vacuum line. Pyridine adsorption was carried out at 403 K. After establishing a pressure of
203 133 Pa at equilibrium, the cell is evacuated at 423 K to remove all physisorbed species. The
204 amount of pyridine adsorbed on the Brønsted and Lewis sites is determined by integrating
205 the band areas at respectively 1545 cm^{-1} and 1454 cm^{-1}. Lewis acidity not was detected for
206 this resin.
207
208 **2.3. Etherification of glycerol with *tert*-butyl alcohol and analysis**
209 The etherification reaction was carried out in a glass autoclave reactor, provided
210 with temperature control, a manometer and stirring control. In order to avoid diffusion
211 limitations, in all experiments the stirring speed was adjusted to 1200 rpm. In previous

studies [10, 32], it was determined that at high rates of agitation, the selectivity towards ethers is higher, while at speeds below 1000 rpm, oligomerization of isobutene can occur. For the etherification reaction of glycerol with *tert*-butyl alcohol, 2.79 g of glycerol, 9.00 g of *tert*-butyl alcohol (glycerol/*tert*-butyl alcohol molar ratio of 0.25) and a constant catalyst loading of 7.5% (with respect to the glycerol mass) was used in all experiments. The reaction temperature was set at 363 K and the samples were taken at different times for 10 h under autogenous pressure, which is the pressure reached inside the reactor by the same reaction system, without establishing a pressure due to an external atmosphere. The pressures reached up to 5 bar. The evolution of the reaction was followed by gas chromatography using a chromatograph model Agilent HP-6890, DB-WAX column and a FID detector and butanol (99%, Sigma Aldrich) as internal standard. The temperature program used consisted of an isotherm at 313 K for 2 minutes, an increase rate of 293 K/min until reaching 513 K, where there was another isotherm for 5 minutes. Glycerol, MTBG (3-*tert*-butoxy-1,2 propanediol and 2-*tert*-butoxy-1,3 propanediol) and DTBG (2,3-di-*tert*-butoxy-1-propanol and 1,3-di-*tert*-butoxy-2-propanol) response factors were determined by calibration performed with standards. MTBG and DTBG (which is not commercially available), were isolated from the products of the etherification reaction by column chromatography (1:9 ethyl acetate/petroleum ether) and identified by ^{1}H NMR.

Glycerol conversion (%), product selectivity (%) and the molar yield (%), were calculated using the following equations [16]:

$$\text{Glycerol conversion (\%)} = \frac{\text{moles of reacted glycerol}}{\text{moles of initial glycerol}} \qquad \text{(eq.1)}$$

$$\text{Product selectivity (\%)} = \frac{\text{moles of obtained product}}{\text{total moles of product}} \qquad \text{(eq. 2)}$$

$$\text{Molar yield (\%)} = \frac{\text{moles of obtained product}}{\text{moles of initial glycerol}} \quad \text{(eq. 3)}$$

The carbon balance with respect to glycerol was close to 97 % for all the catalysts.

3. Results and discussion

3.1. Textural properties

Table 1 reports the BET Surface, the elemental analysis and the acidity achieved from Boehm titration of activated carbons, Amberlyst® 15 (reference catalyst) and graphene oxides. The BET surface area obtained for activated carbon shows that a reduction process leads to a small decrease in the initial value (from 978 to 919 $m^2 g^{-1}$), while the sulfonation process drastically decreases the surface area (224 $m^2 g^{-1}$), probably because of the obstruction of some pores [33]. Amberlyst® 15 features a BET area of 53 $m^2 g^{-1}$, which is characteristic of this resin with pores in the macroporous range comprised between of 40 to 80 nm [34]. Differently, graphene oxide (GO) exhibits low surface areas (5 $m^2 g^{-1}$). The theoretical value for completely exfoliated and isolated graphene sheets is 2600–2700 $m^2 g^{-1}$. Yet, the textural properties of GO in the wet/dispersed state differ significantly from those in the dried state [17], as the restacking of the sheets upon drying leads to a strong decrease in the adsorption capacity [35].

The reduction process using hydrazine dihydrochloride leads to a small increase in surface area by removing some oxygenated groups from the surface (from 5 to 22 $m^2 g^{-1}$), while sulfonation leads to BET areas of less than 11 $m^2 g^{-1}$ for sulfonated reduced GO solid.

The XRD patterns of graphite, pre-oxidized graphite, GO, (GO)R_A, (GO)R_H, and (GO)R_Z-S are shown in **Figure 1**. According to XRD for the pre-oxidized graphite, it shows no

structural changes after treatment with the mixture between concentrated sulfuric acid, potassium persulfate and phosphorus pentoxide, retaining the same very strong [002] peak at 26.57° as the starting graphite, although XPS **(**see XPS analysis below**)** allows to reveal the presence of some oxygenated groups in the surface of this material. For the GO sample a peak at 10.13° is observed which is due to the formation of hydroxyl, epoxy and carboxyl groups ([001] plane). The introduced oxygenated functions increase the interlayer spacing from 0.34 nm in graphite to 0.87 nm in GO, and the stacking height and the layered arrangement was 41 nm with 110 sheets and 10 nm with 12 sheets respectively. After reduction of the GO with ascorbic acid ((GO)R_A), the oxygen- containing functional groups are removed, which lead to shift of the GO peak to 24.33° and a weak [100] band at 43.4º. This feature can be related to the degradation of the layered structure during the exfoliation step and suggests an intermediate crystalline structure between graphite and amorphous carbon that has been named turbostratic structure or random layer lattice structure [29,36]. For this same solid, the interlayer spacing is 0.37 nm and the layered arrangement was 1.13 nm with 3 sheets. The reduction process using hydrazine dihydrochloride ((GO)R_H) not all oxygen groups are eliminated (XPS analysis below), for this reason besides the main peak at 26.18°, a peak at 13.16º is observed, which suggests that part of the initial structure of GO is maintained after the reduction process with this agent. The interlayer spacing is 0.34 nm for graphene oxide reduced by this route and 0.67 nm for the remaining non-reduced graphene oxide. On the other hand, the sulfonation process does not affect the structure of the reduced oxide with Zn/HCl ((GO)R_Z-S) where a [002] peak at 25.25º is predominant. Additionally, it a broad shoulder at 22.23° can be inferred, presumably induced by a bimodal or multimodal character of the interlayer spacing of (GO)R_Z-S powder [37]. The stacking height and the layered arrangement for this sample was 1.41 nm with 4 sheets,

281 respectively. This result confirms the successful exfoliation through the reduction process
282 and with the respective functionalization approaches.
283
284 The Raman spectra of graphite, GO, (GO)R_H and (GO)R_A are shown in the **Figure 2**. These
285 confirm the observations by the XRD patterns *i.e.*, structural modification during the
286 oxidation process from graphite to graphene oxide. The Raman spectrum of graphite
287 displays a strong peak at 1580 cm^{-1}, corresponding to the G-band, which is attributed to the
288 first order scattering of the E_{2g} phonon of the sp^2 carbon-carbon bond [38]. The Raman
289 spectra of GO, shows a slight shift of the G-band to 1584 cm^{-1}. For (GO)R_H and (GO)R_A,
290 the G-band is further shifted to values of 1590 cm^{-1}. The shift of this band could be related
291 to the number of layers present in the material [39]. After oxidation process of the graphite
292 to GO, the D-band develops, which represents the defect sites associated with vacancies
293 and grain boundaries [26, 29] due to extensive oxidation [40]. This D-band (around 1355
294 cm^{-1}) is due to a breathing mode of A_{1g} symmetry involving phonons near the K zone
295 boundary [41].
296
297 The morphological characteristics of the samples were investigated by microscopy. The
298 achieved scanning electron microscopy (SEM) images show that the laminar form of the
299 graphite was not significantly altered by the oxidation processes. The observed corrugation
300 of GO sheets can be attributed to the breaking of the planar polyaromatic structure [26],
301 (**Fig. 3b**). After the reduction process (with ascorbic acid), the restoration of the sheets by
302 *pi*-interactions is evident, while ultrasound treatment, during the preparation of (GO)R_A,
303 leads to irreversible separation of the layers and a completely corrugated morphology is
304 observed (**Fig. 3d**).

The results obtained from SEM convey well with those achieved by transmission electron microscopy (TEM) (**Fig. 4**). The TEM image of graphite presents electron dark areas that indicate the existence of several layers of the polyaromatic structure. Electron clear regions present in GO, indicate much thinner films of few layers of graphene oxide. Additionally, GO sample present sizes of 200 to 500 nm. The reduction with ascorbic acid and subsequent sulfonation does not alter the morphology. Yet, the reduction with hydrazine allows to observe large agglomerations, probably due to the combination of the reduced layers with the remaining graphene oxide which was not reduced (determined by XRD).

The quantitative energy dispersive X-ray spectroscopy (EDS) mapping of (GO)R_H-S and (GO)R_A-S, reveals a homogeneous distribution of -$PhSO_3H$ functionalities, which indicates that these are not exclusively located at the edges [20], (**Figure 4)**. For the functionalization of (GO)R_z with the aryl diazonium salt of the sulfanilic acid, a re-hybridization of the C atoms from sp^2 to sp^3 is required, to form covalent bonds. It is well known that the chemical reduction of graphene oxide generates a substantial amount of defects, including holes in the basal plane, which are allow to increased the amount of grafted -$PhSO_3H$ groups [42].

Elemental analysis

Elemental analysis by combustion was used to investigate the degree of reduction of the powder samples and the degree of sulfonation. **Table 1** summarizes the results of the elemental analysis, in addition to the determination of the C/O and S/C ratios. The obtained graphene oxide (GO) has a C/O ratio of 0.78, which reflects high oxidation in the material with respect to the starting graphite, which features a C/O ratio of 56.64. Through reduction a notable differences in the C/O ratios can be observed. According to our results, the

reduction with Zn/HCl is more effective than with hydrazine hydrochloride and ascorbic acid, generating a C/O ratio of 18.1 against 2.82 and 3.43 for (GO)R_H and (GO)R_Z, respectively. With respect to the S/C ratio, it is possible to observe that the graphene oxide contains residual sulfur, which is due to the oxidizing process in which sulfuric acid was used [43,44]. It has been described that this residual sulfur is present as sulphate species [45] and is lodged within the leaves of GO [42]. These sulphate species is removed during the reduction process, probably due to the restoration of the leaves and the high solubility in water of the sulphate group [46]. Hence, the presence of sulfur in (GO)R_H, (GO)R_Z and (GO)R_A is exclusively due to the functionalization with sulphanilic acid. The S/C ratio in these solids is greatest in (GO)R_A-S, followed by (GO)R_Z-S and (GO)R_H-S. These results thus indicate that the employed GO reduction strategy significantly influences the degree of S-functionalization. Probably the poor agglomeration of the sheets after the reduction with L-ascorbic acid (TEM analysis), promotes the grafting of -PhSO_3H groups on the surface.

The XPS spectrum of the C1s for graphite, shows a predominant peak at 284.4 eV corresponding to sp^2 carbon and a small peak at 286.4 eV corresponding to a very low amount of alcoholic or phenolic C-O-H groups [47] present in the starting material (**Fig. 5a**). The pre-oxidation treatment of graphite with $K_2S_2O_8/P_2O_5$ **(Fig. 5b)** generated a low number of C-O and C=O groups characterized by the low intensity peaks at 286.4 and 287.7 eV, respectively, while the Csp^2 peak at 284.4 eV remains intense. In GO the presence of a high content Csp^3 carbons was determined (284.2 eV), as well as the functional groups C-O-C (286.2 eV), C=O (288.2 eV) and O-C=O (289.5 eV), which confirm the oxidation process (**Fig. 5c**). The reduction of GO by the use of hydrazine dihydrochloride partially restored the aromatic structure of the material, although some

oxygenated groups remain observable, principally C-O-C (286.6 eV), (**Figure 5d)**. During the reduction, parts of the basal planes near the edges are reduced and subsequently snap together due to π - π interactions, thus narrowing the interlayer distance. Consequently, the reducing agent, hydrazine dihydrochloride, is hindered to penetrate further into the interior of the GO particles, presumably leading to the lower degree of reduction [37] and greater agglomeration (TEM images). The reduction of the GO by ascorbic acid, leads to a greater restoration of the aromatic structure compared with the hydrazine dihydrochloride, since the amount of oxygenated groups after the process was much lower (high C/O ratio), (**Table 1**). According to Guo *et al*., L-ascorbic acid significantly reduces the amount of epoxy and hydroxylic groups, which are the most abundant groups in the GO. In addition, a high concentration of L-ascorbic acid, as in our case, can generate oxalic acid and guluronic acids (generated from the decomposition of dehydroascorbic acid) that are able to form hydrogen bonds with residual oxygen groups and prevent π - π interactions of the graphene sheets, which hinders agglomeration [27], (TEM images). The XPS spectrum of (GO)R_Z-S (**Figure 5f)**, show the presence of a negligible amount of oxygenated groups that have been conserved after the functionalization process on (GO)R_z. **Figure 6**, shows the determination of the atomic concentration (%) determined by XPS, where it is possible to corroborate the different oxygenated groups present in the graphene oxide, after the reduction and sulfonation compared to the starting material.

Acidity

The acidity measurements of the samples were correlated with the number of sulfonic groups (sulfur content) present in the surface and corroborated by the Boehm titration (**Table 1)**. This approach has been used in other studies that find concordance between the

results for sulfonated reduced graphene oxide [26,48]. For the activated carbon (AC), the total acidity comprises the sulfonic groups and the original oxygenated groups present in this type of material. According to Cordoba *et al*. [49] activated carbon G60 presents carboxylic acids, anhydrides and lactone groups, which are responsible for its surface acidity (0.71 mmol $[H^+]$ g^{-1}). After the sulfonation process of AC the total acidity increases to 1.76 mmol $[H^+]$ g^{-1}; of which 1.05 mmol $[H^+]$ g^{-1} correspond to the sulfonated grafted groups. The acidity of the GO, in both cases, was influenced by the presence of sulfate groups remaining from the graphite oxidation processes: GO exhibited a total acidity of 0.51 mmol $[H^+]$ g^{-1}, of which 0.45 mmol $[H^+]$ g^{-1} corresponded to the sulfonated groups, which belong to the groups resulting from the functionalization. After the reduction of GO, the disappearance of the remaining sulfate was evidenced (see atop) and the acidity determined by the Boehm titration equals almost to zero, which is due to the few acidic oxygenated groups remaining on the surface of the reduced graphene oxide. Finally, the acidity obtained by titration of Boehm for the sulfonated reduced graphene oxides was similar to the acidity obtained by the correlation of the sulfur present in these catalysts.

3.2. Etherification of glycerol with *tert*-butyl alcohol

According to our previous work [16], we determined the thermodynamics of the etherification of glycerol with *tert*-butyl alcohol by the use of discontinuous reactors at 363 K under autogenous pressure. The etherification of glycerol and *tert*-butyl alcohol is a reaction limited by a thermodynamic equilibrium. In our experimental conditions the maximum glycerol conversion expected is 80%.

Kinetic model

To determine the partial order of the reaction between glycerol (Gly) and *tert*-butyl alcohol (TBA), the variation of the initial reaction rate and the concentration of the reactants were studied. For this, the catalysts (AC)-S and (GO)R_A-S were used at 363 K and were calculated by the natural logarithm of the rate equation [16]. The initial rate were measured in a series of experiments at different initial concentration of glycerol ranged from $2.0x10^{-4}$ to $1.0x10^{-3}$ mol cm^{-3} with a molar ratio *tert*-butyl alcohol/glycerol from 10 to 40. In these conditions, the concentration of the exceeding reactant can be considered as almost invariant. The slope of the linear regression in **Fig. 7** of the $\ln r_0$ plot as a function of $\ln[Gly]_0$ corresponds to the partial order with respect to Gly. Additionally, experiments were carried out where the concentration of Gly was maintained constant and the TBA concentration was varied from $4.0x10^{-4}$ to $2.0x10^{-3}$ mol cm^{-3}. The partial kinetic orders for (AC)-S with respect to glycerol was 0.16, while the order for TBA was 0.84. For the catalyst (GO)R_A-S, the order obtained with respect to glycerol was 0.42, while for the TBA 1.60. These results agree with those obtained by Frusteri *et al.*, [50] who evaluated the partial orders of the solid-acid resin Amberlyst® 15 in the glycerol etherification which were found to be of 0.3 with respect to Gly and an order of 1.7 with respect to *tert*-butyl alcohol, suggesting that the etherification reaction occurs through fast protonation of TBA on the acid sites forming a tertiary carbocation able to react with glycerol strongly adsorbed on the catalyst surface.

These results further confirm the Langmuir-Hinshelwood (LH) as most suitable kinetic model as indicated by Kiatkittipong *et al*. [51]. The apparent activation energy of the Amberlyst® 15 was 63 kJ mol^{-1}, which is very close to the values calculated in other kinetic studies for this catalyst [52].

425 ***Activity and stability***

426 In **figure 8**, the glycerol conversion was compared as a function of the reaction time
427 for following catalysts: (AC)-S, (AC)R_H-S and Amberlyst® 15 (reference catalyst [14, 51]),
428 (GO), (GO)-S, (GO)R_H-S, (GO)R_Z-S, (GO)R_A-S. By employing A-15 conversion increases
429 rapidly and reaches a plateau at 64% within 1 h. The plateau is 16% lower than the
430 predicted equilibrium value (80%), which indicates that conversion is hampered by
431 deactivation of the sulfonic resin, probably due to a product inhibition effect, *e.g*. by H_2O
432 [16]. As expected, graphite and AC as catalysts do not allow to observe glycerol conversion
433 (**Table 2**). Although these solids feature oxygenated groups (graphite and AC) the acidity
434 that these groups confer is to weak to promote etherification. Sulfonated AC, permits to
435 reach a glycerol conversion of 35%, which suggests that the presence of sulfonated groups
436 promotes the reaction. Additionally, GO was tested as catalyst. As evidences through XPS
437 GO contains oxygenated groups on the surface, as determined by the Boehm titration
438 (**Table 1**), which acidity is low to promote etherification. Additionally GO contained a
439 substantial amount of sulphate species from the preparation process, which could confer the
440 appropriate acid strength to carry out the reaction. Indeed, one strategy to functionalize
441 graphene with acid groups is its direct immersion in concentrated sulfuric acid [53]. The
442 glycerol conversion achieved with GO amounts to 19%.
443
444 The results of the catalytic etherification of glycerol with *tert*-butyl alcohol was
445 further compared in terms of initial activity (A_0), where possible deactivation does not
446 occur. A_0 was obtained from the slope of the tangent at zero time fitted to the conversion
447 vs. time graphs (**Figure 8).** The initial activity of the catalyst based on sulfonated reduced
448 graphene oxide is very close to the activity of the sulfonic resin A-15, (**Table 2**), which can

449 be related to the fact that both the Amberlyst® 15 and the graphene-based solids contain the
450 same acidic surface moieties (*i.e.* -$PhSO_3H$). Additionally, both types of materials present
451 the absence of micropores as in the case of activated carbons, where substantially lower
452 initial activities are observed. The initial activity (A_0) of the catalysts evaluated was related
453 to the acidity obtained for each catalyst (**Figure 9**). It can be seen that, in general, there is a
454 correlation for catalysts based on graphene oxide, where the initial activity depends on the
455 concentration of acid. For catalysts based on activated carbon, the activity does not increase
456 with increasing acid concentration.

457 The recyclability of (AC)-S and (GO)R_A-S was investigated through comparing the
458 molar yields toward MTBG and DTBG. After 3 recycling cycles the glycerol conversion
459 using (GO)R_A-S, decreases by 11% and the molar yield towards *poly*-substituted ethers
460 decreases of than 50% (from 22 to 10%), **Fig. 10**. As similar result is observed for (AC)-S,
461 although in this case the conversion decreases only by 1%. In the case the catalysts are
462 regenerated through ethanol washing using Soxhlet, the initial conversion can be recovered
463 for all catalysts. This suggests the deactivation occurs through adsorption of reagents and
464 products on the active sites. This was evidenced through analyzing the ethanol fraction
465 from the washing cycle by gas chromatography. Here the main peaks are glycerol and
466 MTBG. Hence, it is possible to recover the initial activity by means of solvent washing.
467 Elemental analysis was used to verify the elemental ratio in the sulfonated reduced
468 graphene oxide catalysts after use. The results showed that the proportions of carbon,
469 oxygen and sulfur elements do not have noticeable changes. These observations indicate
470 that sulfonated reduced graphene oxide is a stable and easily recyclable catalyst for
471 etherification with glycerol.
472

Selectivity

The etherification of glycerol with *tert*-butyl alcohol is a reaction of successive routes that produces water as a by-product and five different alkyl ethers, which are: MTBG (3- *tert*-butoxy-1,2 propanediol and 2-*tert*-butoxy-1,3 propanediol), DTBG (2,3-di-*tert*-butoxy-1-propanol and 1,3-di-*tert*-butoxy-2- propanol) and TTBG (tri-*tert*-butoxy-propane). Side reactions can occur such as the dehydration of *tert*-butyl alcohol to isobutylene (IB) followed of its dimerization. Under the performed reaction conditions, no diisobutylene was detected as the isobutylene yield estimated from the autogenous pressure is negligible (<1%) [16]. **Fig. 11** compares MTBG (primary product) and the *poly*-substituted ethers (DTBG and TTBG) molar yields as function of the overall glycerol conversion employing Amberlyst® 15, and sulfonated reduced graphene oxide-based catalyst. **Table 2** reports conversion and product selectivity obtained after 10 h of reaction.

Using A-15, the yield of the primary product (MTBG) reaches a maximum at ca. 60% glycerol conversion. The DTBG (secondary product) is starting to be formed at 23 % glycerol conversion (extrapolated value at zero conversion). After 10 h of reaction, one quarter of the products are composed of DTBG, whereas the yield of TTBG (ternary product) is negligible (0.3%). For the catalyst (AC)-S, the formation of DTBG occurs at low conversion (~20%). This is related to the high microporosity of activated carbon in which the reaction in sterically limited spaces can have a major impact on selectivity. In a previous study we have indeed observed that molecular shape selectivity and confinement effect in zeolites have a major effect on product selectivity in the glycerol etherification [16].

For catalysts based on sulfonated reduced graphene oxide, the selectivity obtained towards DTBG depends on the synthesis strategy. Catalysts obtained through hydrazine

497 dihydrochloride and ascorbic acid ((GO)R_H-S and (GO)R_A-S) allow to achieve selectivities
498 toward DTBG of 29 and 27%, respectively, after 10 h of reaction (**Table 2**). In fact, these
499 solids do not present any porosity and, therefore, the formation of DTBG is observed only
500 after a glycerol conversion of 24%. (**Fig. 11**). Although the conversion after 10 h of
501 reaction is similar for the three catalysts ((GO)R_H-S, (GO)R_Z-S and (GO)R_A-S), the
502 selectivity obtained with (GO)R_Z-S differs significantly and reaches merely 12% DTBG
503 (**Table 2**). Further, for the catalyst (GO)R_Z-S, it is observed that DTBGs are formed upon
504 reaching a glycerol conversion of 54%. These large differences in selectivity are related to
505 the amount of oxygen groups in these catalysts, which influence the
506 hydrophobic/hydrophilic (H/H) balance. According to Huang *et al*., the hydrophobicity of
507 graphene oxide increases with the degree of reduction or elimination of oxygenated groups
508 [54]. On the other hand, Mitra and Azizighannad evaluated the hydrophobicity index of the
509 graphene oxides reduced with Zn/HCl, where using different amounts of Zn, they obtained
510 graphene oxide with different percentages of oxygen. The results of their study also
511 corroborate that a lower oxygen content leads to a higher hydrophobicity index [55].
512 Indeed, the H/H balance on selectivity has previously been discussed for zeolites for the
513 glycerol etherification with *tert*-butyl alcohol [16, 56, 57]. According to the results of this
514 study, the H/H balance also affects the selectivity in graphene oxide-based catalysts. It is
515 possible to suggest that there is a synergy between the active sites (sulfonic groups) and the
516 amount of oxygen groups remaining in the sulfonated reduced graphene oxides.
517 Oxygenated groups can serve as adsorption sites for reagents and products, promoting the
518 consecutive reaction of MTBG to DTBG and TTBG. In the case of graphene oxide, which
519 mostly contains only sulfonic groups on the surface and very few oxygenated groups -as in

520 the case of (GO)R_Z-S, a high conversion of glycerol can be generated, but the selectivity
521 obtained towards *poly*-substituted ethers could be low.
522
523 **4. Conclusion**
524 Sulfonated reduced graphene oxide has been obtained through different methods of
525 synthesis previously reported in the literature and then tested in the glycerol etherification
526 with *tert*-butyl alcohol. The results indicate that it is important to synthesize nanometric
527 graphene oxide and prior to acid functionalization, the reducing agent must be correctly
528 selected. In our study, the route that was favored was the reduction with ascorbic acid,
529 converting the process into a green synthesis by preventing the use of typical toxic reducing
530 agents such as hydrazine. The sulfonation using diazotization is an easy and effective route
531 to functionalize the reduced graphene oxide, since it generates a homogeneous dispersion in
532 the carbon skeleton. The results of activity of this type of catalysts, show better results than
533 those achieved with the reference catalyst Amberlyst® 15. The selectivity towards *poly*-
534 substituted ethers is influenced by the synergy between the remaining oxygenated species
535 after the reduction process and the grafted sulfonic groups. As far as recyclability is
536 concerned, these catalysts have shown to be stable and easily regenerable (through ethanol
537 washing), converting them into efficient solids in acid reactions in which the formation of
538 water as a by-product is observed, such as the glycerol etherification with *tert*-butyl
539 alcohol.
540
541 **Acknowledgements**

C. Miranda thanks Colciencias for the financial support provided for doctoral formation through the 617 convocation. The authors further acknowledge financial support from the European Union (ERDF) and "Région Nouvelle Aquitaine".

References

[1] M. Pagliaro, R. Ciriminna, H. Kimura, M. Rossi and C. Della Pina, *Angew. Chem. Int. Ed. Engl.* 46 (2007) 4434-4440.

[2] C. Len and R. Luque, *Sustain. Chem. Process.* 2 (2014) 1-10.

[3] J. F. Izquierdo, M. Montiel, I. Palés, P. R. Outón, M. Galán, L. Jutglar, M. Villarrubia, M. Izquierdo, M. P. Hermo and X. Ariza, *Renew. Sust. Energ. Rev.* 16 (2012) 6717-6724.

[4] M. Sutter, E. D. Silva, N. Duguet, Y. Raoul, E. Metay and M. Lemaire, *Chem. Rev.* 115 (2015) 8609-8651.

564 [5] C. Cannilla, G. Bonura, L. Frusteri and F. Frusteri, *Chem. Eng. J.* 282 (2015) 187-
565 193.

566 [6] C. Cannilla, G. Bonura, L. Frusteri and F. Frusteri, *Cent. Eur. J. Chem.* 12 (2014)
567 1248–1254.

568 [7] L. Frusteri, C. Cannilla, G. Bonura, A. L. Chuvilin, S. Perathoner, G. Centi and F.
569 Frusteri, *Catal. Today*. 277 (2016) 68-77.

570 [8] K. Klepáčová, D. Mravec, A. Kaszonyi. and M. Bajus, *Appl. Catal., A*, 328 (2007)
571 1-13.

572 [9] J. A. Melero, G. Vicente, G. Morales, M. Paniagua, J. M. Moreno, R. Roldán, A.
573 Ezquerro and C. Pérez, *Appl. Catal., A*, 346 (2008) 44-51.

574 [10] R. S. Karinen and A. O. I. Krause, *Appl. Catal. A*, 306 (2006) 128-133.

575 [11] E. Vlad, C. S. Bildea and G. Bozga, *ScientificWorldJournal*, 2012 (2012) 180617.

576 [12] C. Cannilla, G. Bonura, L. Frusteri and F. Frusteri, *Environ. Sci. Technol*., 48 (2014)
577 6019-6026.

578 [13] Theodore, E. and K.R. Edlund, *Process and product relating to tertiary ethers*,
579 1934.

580 [14] K. Klepáčová, D. Mravec and M. Bajus, *Appl. Catal., A*, 294 (2005) 141-147.

581 [15] K. Y. Nandiwale, S. E. Patil and V. V. Bokade, *Energy Technol.* 2 (2014) 446-452.

[16] C. Miranda, J. Urresta, H. Cruchade, A. Tran, M. Benghalem, A. Astafan, P. Gaudin, T. J. Daou, A. Ramírez, Y. Pouilloux, A. Sachse and L. Pinard, *J. Catal.*, 365 (2018) 249-260.

[17] M. M. Antunes, P. A. Russo, P. V. Wiper, J. M. Veiga, M. Pillinger, L. Mafra, D. V. Evtuguin, N. Pinna and A. A. Valente, *ChemSusChem*, 7 (2014) 804-812.

[18] J. Janaun and N. Ellis, *J. Appl. Sci.*, 10 (2010) 2633-2637.

[19] T. S. Galhardo, N. Simone, M. Gonçalves, F. C. A. Figueiredo, D. Mandelli and W. A. Carvalho, *ACS Sus. Chem. Eng.*, 1 (2013) 1381-1389.

[20] J. Ji, G. Zhang, H. Chen, S. Wang, G. Zhang, F. Zhang and X. Fan, *Chem. Sci.* 2 (2011) 484-487.

[21] M. Brahmayya, S. A. Dai and S. Y. Suen, *Sci. Rep.* 7 (2017) 4675.

[22] L. Wang, D. Wang, S. Zhang and H. Tian, *Catal. Sci. Technol.* 3 (2013) 1194-1197.

[23] K. K. Praveen, K. Prashant, N. Ponnnekanti and L. J. Suman, *Lett. Org. Chem.* 15 (2018) 508-514.

[24] J. Zhou, Y. Wang, X. Guo, J. Mao and S. Zhang, *Green Chem.* 16 (2014) 4669-4679.

[25] N. I. Kovtyukhova, P. J. Ollivier, B. R. Martin, T. E. Mallouk, S. A. Chizhik, E. V. Buzaneva and A. D. Gorchinskiy, *Chem. Mater.* 11 (1999) 771-778.

[26] W. S. Hummers and R. E. Offeman, *J. Am. Chem. Soc.* 80 (1958) 1339-1339.

[27] J. Zhang, H. Yang, G. Shen, P. Cheng, J. Zhang and S. Guo, *Chem. Commun.*, 46 (2010) 1112-1114

[28] X. Mei and J. Ouyang, *Carbon*, 49 (2011) 5389-5397.

[29] N. Oger, Y. F. Lin, C. Labrugère, E. Le Grognec, F. Rataboul and F.-X. Felpin, *Carbon*, 96 (2016) 342-350.

[30] A. T. Quitain, Y. Sumigawa, E. G. Mission, M. Sasaki, S. Assabumrungrat and T. Kida, *Energy Fuels*, 32 (2018) 3599-3607.

[31] K. Nakajima and M. Hara, *ACS Catalysis*, 2 (2012) 1296-1304.

[32] M. D. González, P. Salagre, M. Linares, R. García, D. Serrano and Y. Cesteros, *Appl. Catal. A*, 473 (2014) 75-82.

[33] X. Y. Liu, M. Huang, H. L. Ma, Z. Q. Zhang, J. M. Gao, Y. L. Zhu, X. J. Han and X. Y. Guo, *Molecules*, 15 (2010) 7188-7196.

[34] R. Kunin, E. A. Meitzner, J. A. Oline, S. A. Fisher and N. Frisch, *Ind. Eng. Chem. Prod. Res. Dev.* 1 (1962) 140-144.

[35] R. L. Whitby, V. M. Gun'ko, A. Korobeinyk, R. Busquets, A. B. Cundy, K. Laszlo, J. Skubiszewska-Zieba, R. Leboda, E. Tombacz, I. Y. Toth, K. Kovacs and S. V. Mikhalovsky, *ACS Nano*, 6 (2012) 3967-3973.

[36] B. Manoj and A. Kunjomana, *Int. J. Electrochem. Sci.*, 7 (2012) 3127-3134.

[37] S. Park, J. An, J. R. Potts, A. Velamakanni, S. Murali and R. S. Ruoff, *Carbon*, 49 (2011) 3019-3023.

[38] R. Saito, M. Hofmann, G. Dresselhaus, A. Jorio and M. S. Dresselhaus, *Adv. Phys.* 60 (2011) 413-550.

[39] S. S. Nanda, M. J. Kim, K. S. Yeom, S. S. A. An, H. Ju and D. K.Yi, *TrAC, Trends Anal. Chem.* 80 (2016) 125-131.

[40] S. Stankovich, D. A. Dikin, R. D. Piner, K. A. Kohlhaas, A. Kleinhammes, Y. Jia, Y. Wu, S. T. Nguyen and R. S. Ruoff, *Carbon*, 45 (2007) 1558-1565.

[41] A. C. Ferrari and J. Robertson, *Phys. Rev. B*, 61 (2000) 14095-14107.

[42] S. Eigler and A. Hirsch, *Angew. Chem. Int. Ed.*, 53 (2014) 7720-7738.

[43] S. Zhu, C. Chen, Y. Xue, J. Wu, J. Wang and W. Fan, *ChemCatChem*, 6 (2014) 3080-3083.

[44] X. Gao, S. Zhu and Y. Li, *Catal. Commun.* 62 (2015) 48-51.

[45] G. Wang, B. Wang, J. Park, J. Yang, X. Shen and J. Yao, *Carbon*, 47 (2009) 68-72.

[46] M. Brahmayya, S. A. Dai and S.-Y. Suen, *Sci Rep.* 7 (2017) 4675.

[47] C. Hontoria-Lucas, A. J. López-Peinado, J. d. D. López-González, M. L. Rojas-Cervantes and R. M. Martín-Aranda, *Carbon*, 33 (1995) 1585-1592.

[48] A. V. Nakhate and G. D. Yadav, *ACS Sustainable Chem. Eng.* 4 (2016) 1963-1973.

[49] M. Cordoba, C. Miranda, C. Lederhos, F. Coloma-Pascual, A. Ardila, G. Fuentes, Y. Pouilloux and A. Ramírez, *Catalysts*, 7 (2017) 384.

[50] F. Frusteri, F. Arena, G. Bonura, C. Cannilla, L. Spadaro and O. Di Blasi, *Appl. Catal., A*, 367 (2009) 77-83.

[51] W. Kiatkittipong, P. Intaracharoen, N. Laosiripojana, C. Chaisuk, P. Praserthdam and S. Assabumrungrat, *Comput. Chem. Eng.* 35 (2011) 2034-2043.

[52] M. Sharma, R. K. Wanchoo, and A. P. Toor, *Ind. Eng. Chem. Res.* 53 (2014) 2167-2174

[53] M. Mirza-Aghayan, M. M. Tavana and R. Boukherroub, *Ultrason. Sonochem.* 29 (2016) 371-379.

[54] L. J. Cote, J. Kim, V. C. Tung, J. Luo, F. Kim and J. Huang, *Pure Appl. Chem*., 83 (2011) 95–110.

[55] S. Azizighannad and S. Mitra, *Sci. Rep.*, 8 (2018) 1-8.

[56] P. M. Veiga, A. C. L. Gomes, C. O. Veloso and C. A. Henriques, *Appl. Catal. A*, 548 (2017) 2-15.

[57] M. D. González, Y. Cesteros and P. Salagre, *Appl. Catal. A*, 450 (2013) 178-188.

List of tables and figures

Table 1. Textural and acidic properties of Amberlyst® 15, graphene oxide and sulfonated reduced graphene oxide.

Table 2. Glycerol etherification with *tert*-butyl alcohol: conversion and selectivity after 10 h, initial activity (A_0) and TOF obtained on activated carbon, Amberlyst®15, GO and sulfonated reduced graphene oxide.

Figure 1. XRD patterns of graphite, preoxidated graphite, (GO), (GO)R_A, (GO)R_H and (GO)R_Z-S.

Figure 2. Raman spectra of graphite, (GO), (GO)R_H, and (GO)R_A.

Figure 3. SEM images of: a) graphite; b) (GO), c) (GO)R_A; d) (GO)R_A-S.

Figure 4. Transmission electronic images of the samples and EDS mapping showing the spatial distribution of C and S of (GO)R_H-S and (GO)R_A-S.

Figure 5. XPS spectra for graphite, a); pre-oxidized graphite, b); (GO), c); (GO)R_H, d); (GO)R_A, e); (GO)R_Z-S, f).

Figure 6. Atomic concentration (%) determined by XPS of graphite, pre-oxidized graphite, (GO), (GO)R_H, (GO)R_A and (GO)R_Z-S.

Figure 7. Kinetical study of (AC)-S, a), and (GO)R_A-S, b).

Figure 8. Glycerol conversion as a function of reaction time. (AC)-S, (AC)R_H-S and Amberlyst®15, a); Catalysts based on GO, b). Test carried out at 363 K, 1200 rpm, autogenous pressure, 7,5% of catalyst (referred to glycerol mass) and glycerol/*tert*-butyl alcohol molar ratio of 0.25.

Figure 9. Correlation of the initial activity with the acidity of the catalysts based on GO, AC and Amberlyst® 15

Figure 10. Results of recycling experiments for (GO)R_A-S, a) and (AC)-S, b).

Figure 11. Molar yields into MTBG, DTBG and TTBG as a function of glycerol conversion for catalyst based on sulfonated reduced GO compared to A-15.

Table 1. Textural and acidic properties of Amberlyst®15, graphene oxide and sulfonated reduced graphene oxide.

Catalyst	S_{BET}	Elemental Analysis (%)			Acidity (mmol $[H^+]$ g^{-1})	C/O ratio	S/C ratio
		C	O	S			x10^{-2}
(AC)	978	73.16	24.89	0.00	0.71	3.92	--
(AC)-S	224	67.75	26.29	3.35	1.05 (1.76)[c]	3.44	1.85
(AC)R_H	919	79.39	19.19	0.00	--	5.52	--
(AC)R_H-S	163	68.70	25.33	3.94	1.23	3.62	2.15
A-15	53	-	-	-	2.37[a]		
Graphite	-	97.70	2.30	0.00	--	56.64[b]	--

(GO)	5	35.47	60.29	1.45	0.45 (0.51)[c]	0.78	1.53
(GO)-S		46.99	47.27	2.37	0.74 (0.70)[c]	1.33	1.89
$(GO)R_H$	22	66.40	31.40	0.00	--	2.82	--
$(GO)R_Z$		93.16	6.86	0.00	--	18.1	--
$(GO)R_A$	14	70.96	27.59	0.00	--	3.43	--
$(GO)R_H$-S	11	60.14	34.82	3.29	1.03 (1.05)[c]	2.30	2.05
$(GO)R_Z$-S	10	85.13	10.15	4.72	1.48 (1.37)[c]	11.2	2.08
$(GO)R_A$-S	7	55.86	35.01	6.88	2.15 (2.12)[c]	2.13	4.62

[a] Measured by Pyr-IR adsorption. [b] Measured by XPS. [c] In parenthesis = acidity determined by Boehm titration.

Table 2. Glycerol etherification with *tert*-butyl alcohol: conversion and selectivity after 10 h, initial activity (A^0) and TOF obtained on Amberlyst® 15 (A-15), activated carbon, graphene oxide and sulfonated reduced graphene oxide.

Catalyst	Conv. (%)	Selectivity (%)		$A^0_{glycerol}$ (mol h^{-1} g^{-1}) **x 10^4**	TOF[a] (h^{-1}) **x 10^2**
		MTBG	DTBG		
(AC)	0	0	0	--	--
(AC)-S	35	80	20	1.45	14
$(AC)R_H$-S	31	86	14	1.28	10
A-15	64	75	25 (0.3)	15.00	63
Graphite	0	0	0	--	--
(GO)	19	100	0	5.00	111
(GO)-S	50	78	22 (0.2)	10.53	202

$(GO)R_H$-S	73	71	29 (0.7)	14.02	107
$(GO)R_Z$-S	76	88	12 (0.1)	12.71	194
$(GO)R_A$-S	77	73	27 (0.5)	15.89	74

Reaction conditions: 7.5 wt.% of catalyst (referred to glycerol mass), glycerol/*tert*-butyl alcohol molar ratio = 0.25, reaction temperature = 363 K, reaction time = 10 h, stirring = 1200 rpm. MTBG: glycerol *mono*-ethers; DTBG: glycerol *di*-ethers (glycerol *tri*-ether in parenthesis). [a] Turnover frequency per Brønsted acid sites.

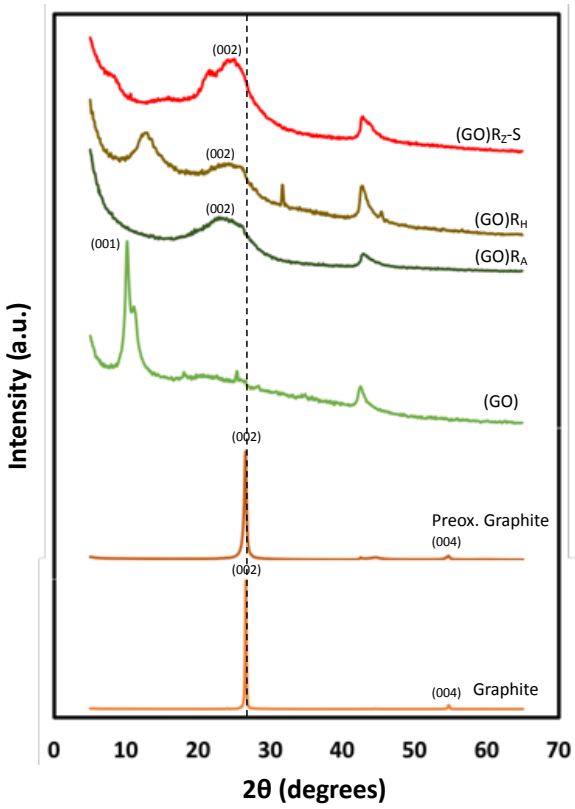

Figure 1. XRD patterns of Graphite, preoxidated graphite, GO, $(GO)R_A$, $(GO)R_H$ and $(GO)R_Z$-S.

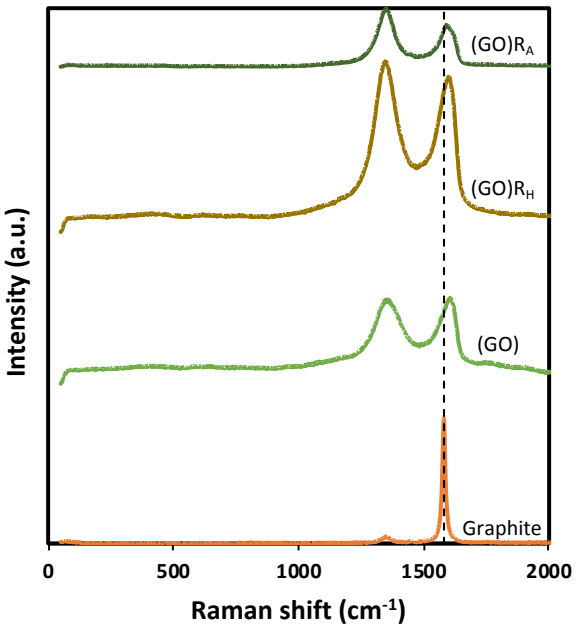

Figure 2. Raman spectra of graphite, (GO), $(GO)R_H$ and $(GO)R_A$.

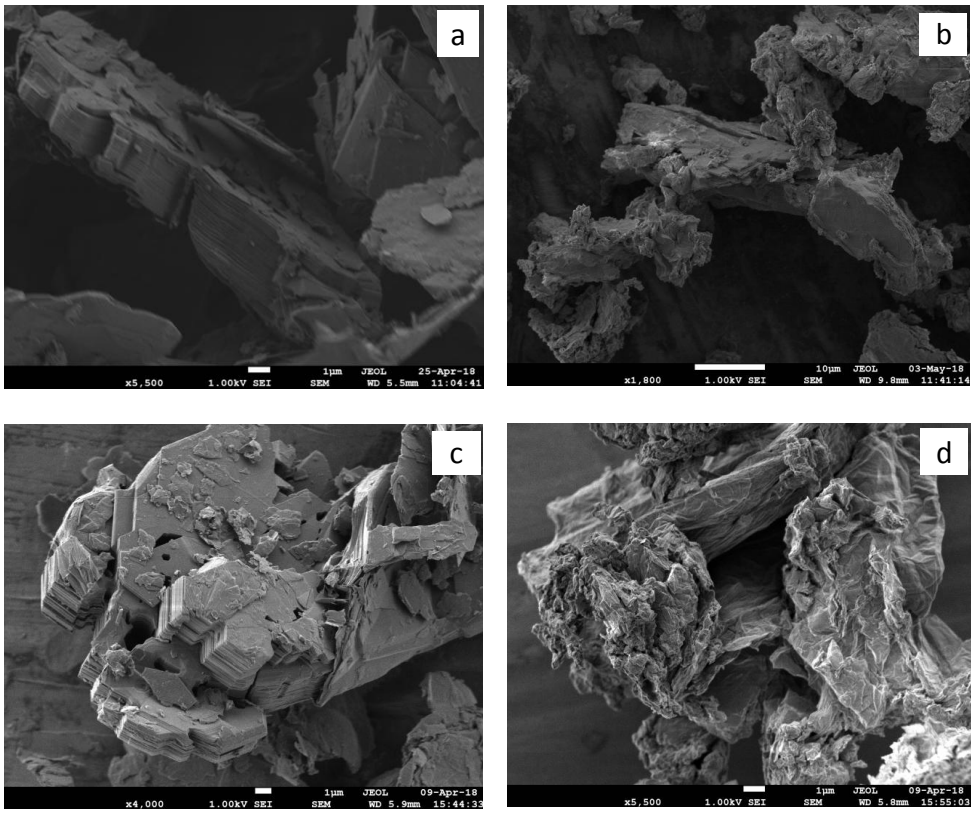

765 **Figure 3**. SEM images of: a) graphite; b) (GO), c) (GO)R_A; d) (GO)R_A-S

766

767

768

769

770

771

772

773

774

775

776

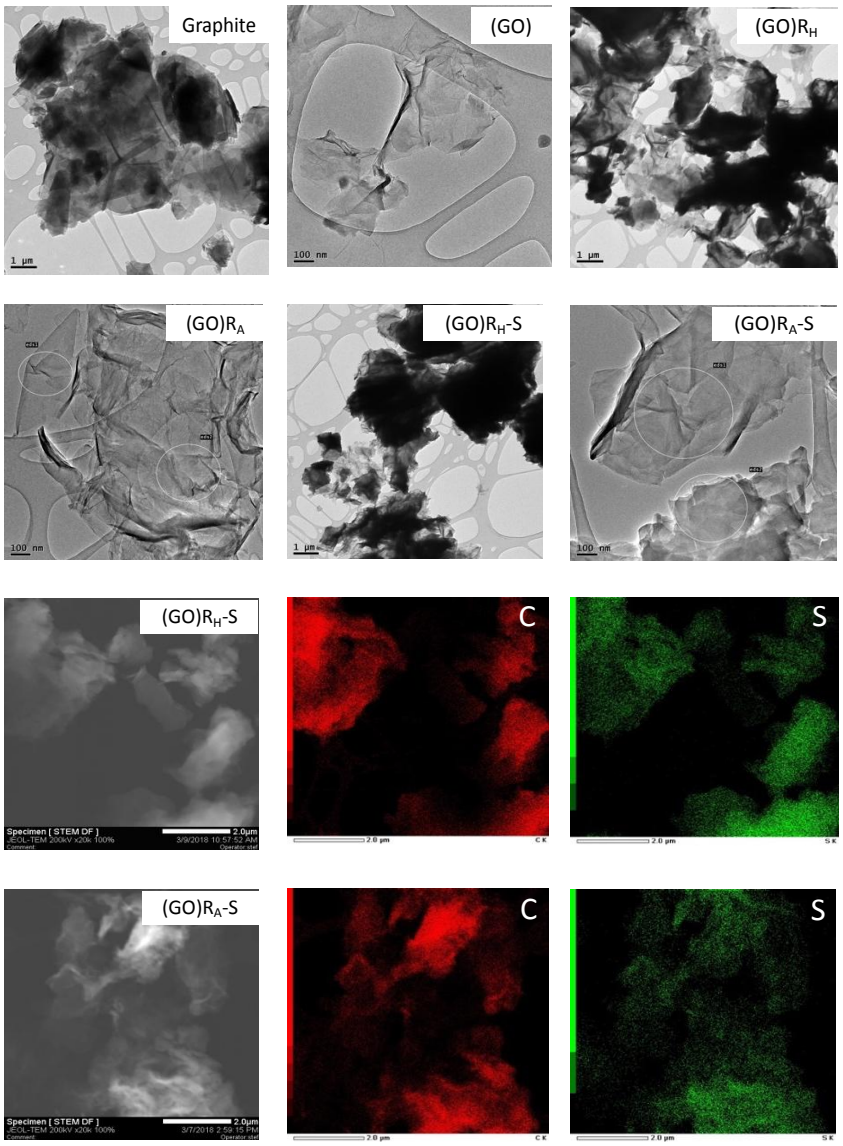

Figure 4. Transmission electronic images of the samples and EDS mapping showing the spatial distribution of C and S of $(GO)R_H$-S and $(GO)R_A$-S.

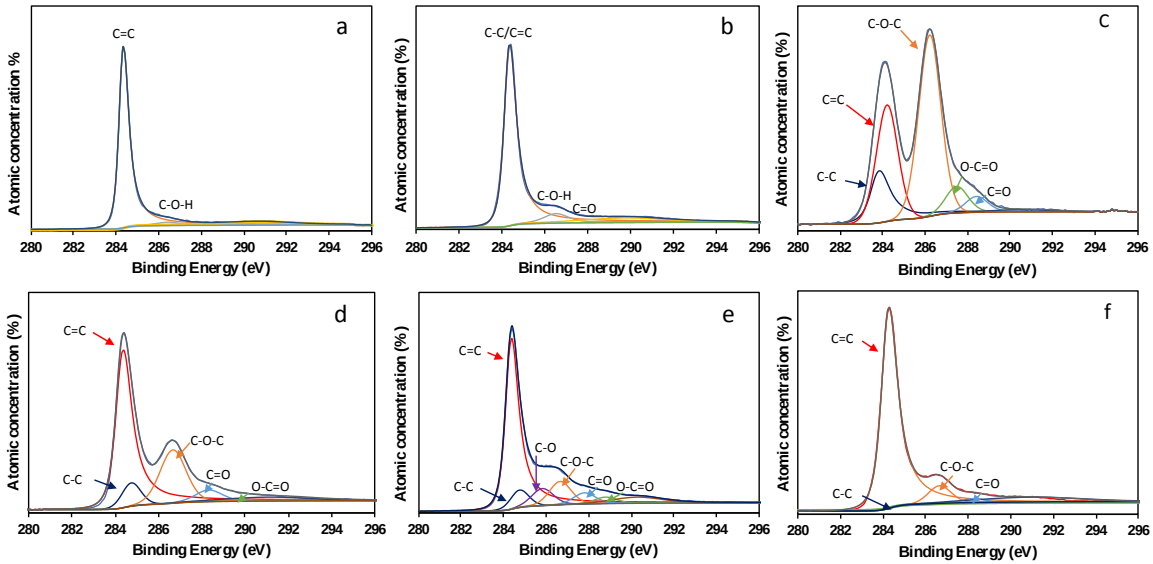

Figure 5. XPS spectra for graphite, a); pre-oxidized graphite, b); (GO), c); (GO)R_H, d); (GO)R_A, e); (GO)R_Z-S, f).

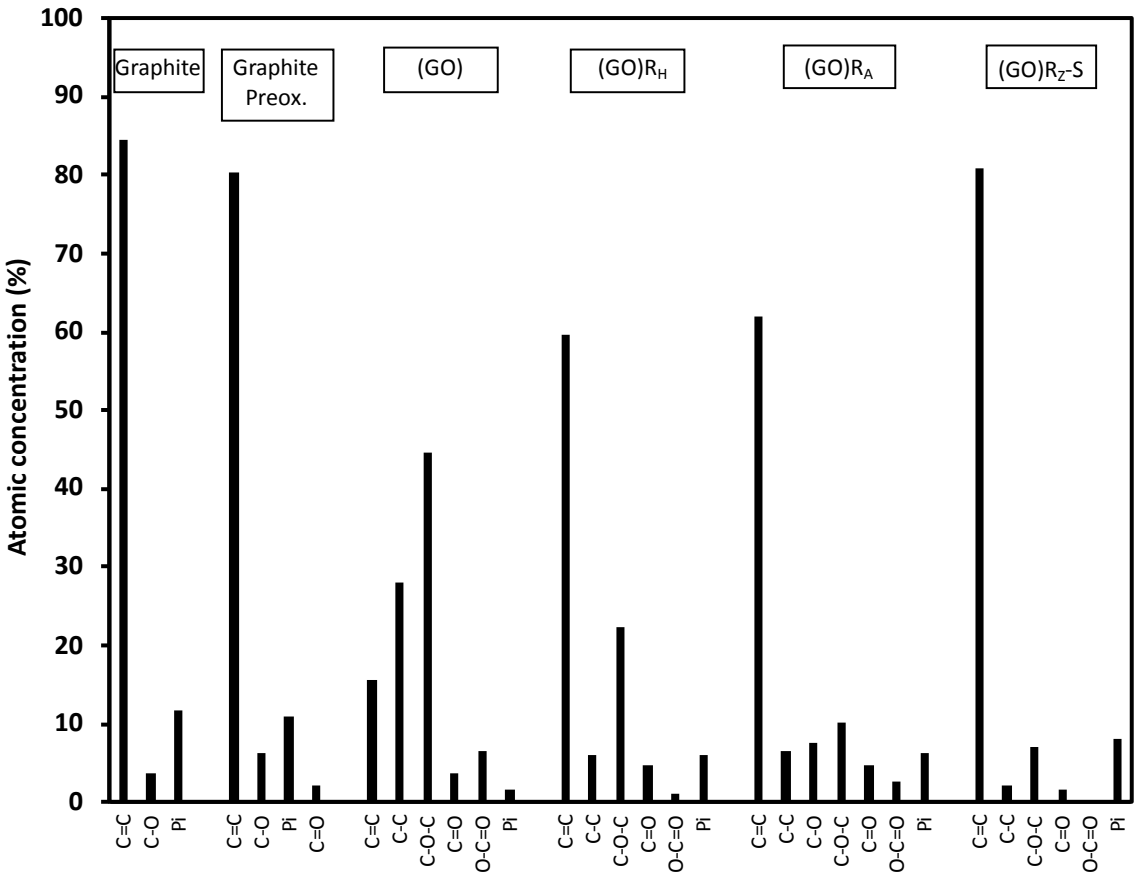

796

797 **Figure 6.** Atomic concentration (%) determined by XPS of graphite, pre-oxidized graphite,

798 (GO), (GO)R_H, (GO)R_A and (GO)R_Z-S.

799

800

801

802

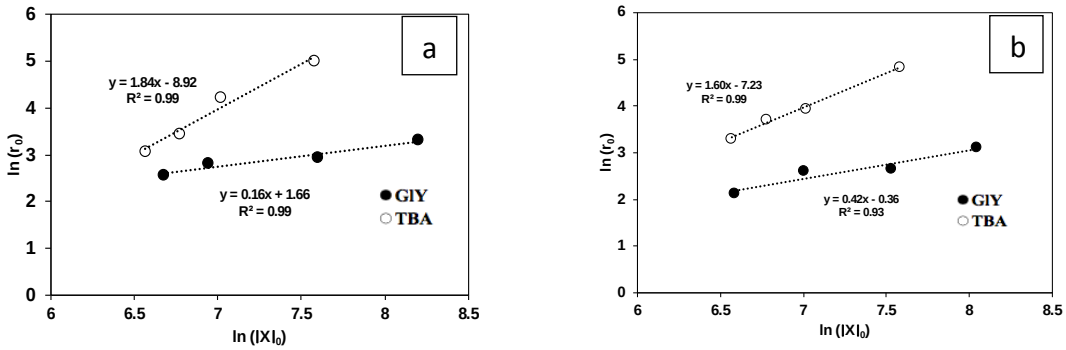

Figure 7. Kinetical study of (AC)-S, a) and (GO)R_A-S, b).

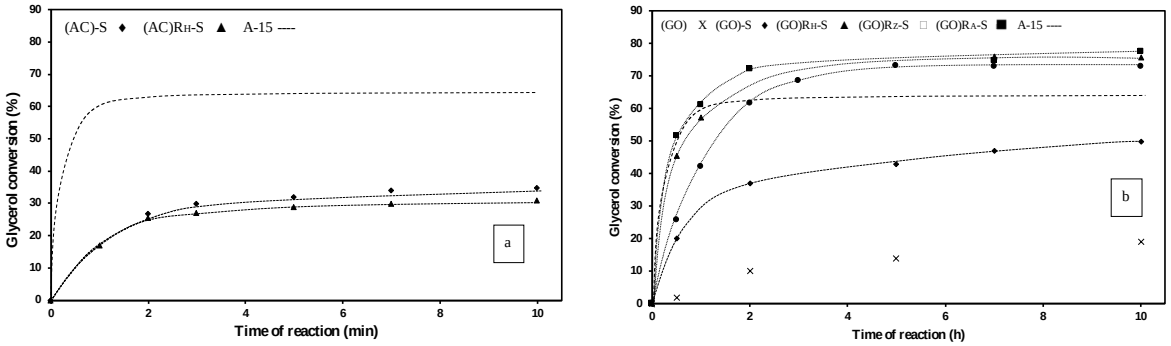

822

823 **Figure 8.** Glycerol conversion as a function of reaction time. (AC)-S, (AC)R_H-S and
824 Amberlyst® 15 (A-15), a); Catalysts based on (GO), b). Test carried out at 363 K, 1200
825 rpm, autogenous pressure, 7,5 % of catalyst (referred to glycerol mass) and glycerol/*tert*-
826 butyl alcohol molar ratio of 0.25.

827

828

829

830

831

832

833

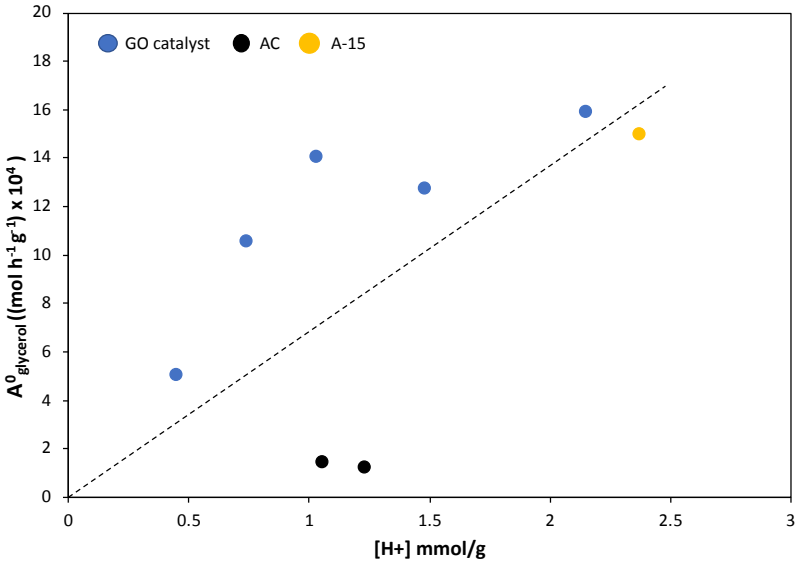

834

835 **Figure 9.** Correlation of the initial activity with the acidity of the catalysts based on GO,

836 AC and Amberlyst® 15.

837

838

839

840

841

842

843

844

845

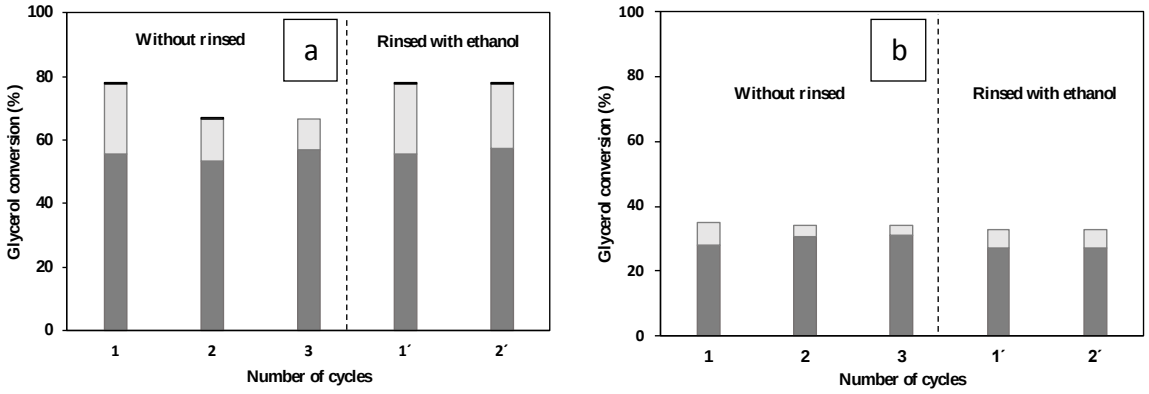

Figure 10. Results of recycling experiments for (GO)R_A-S, a) and (CA)-S, b).

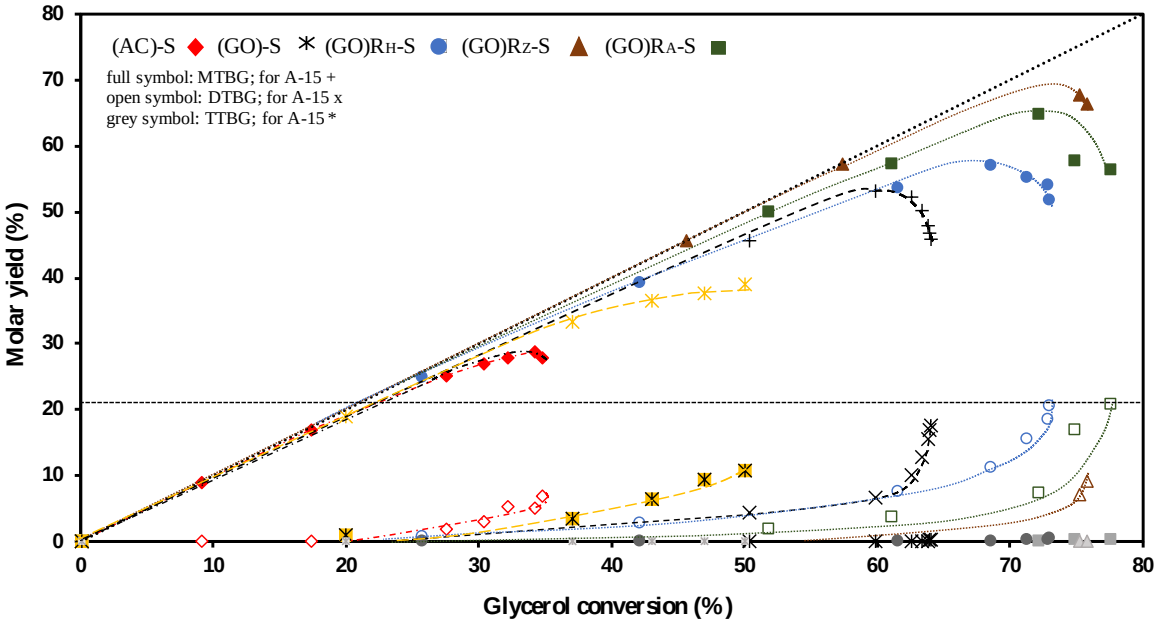

Figure 11. Molar yields into MTBG, DTBG and TTBG as a function of glycerol conversion for catalyst based on sulfonated reduced GO, compared to A-15 and (AC)-S.

Supplementary information

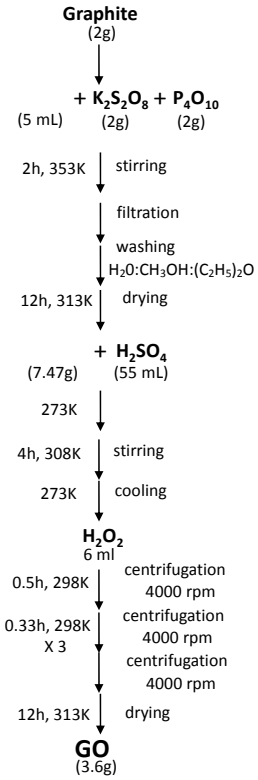

Figure S1. Diagram of synthesis of the graphene oxide.

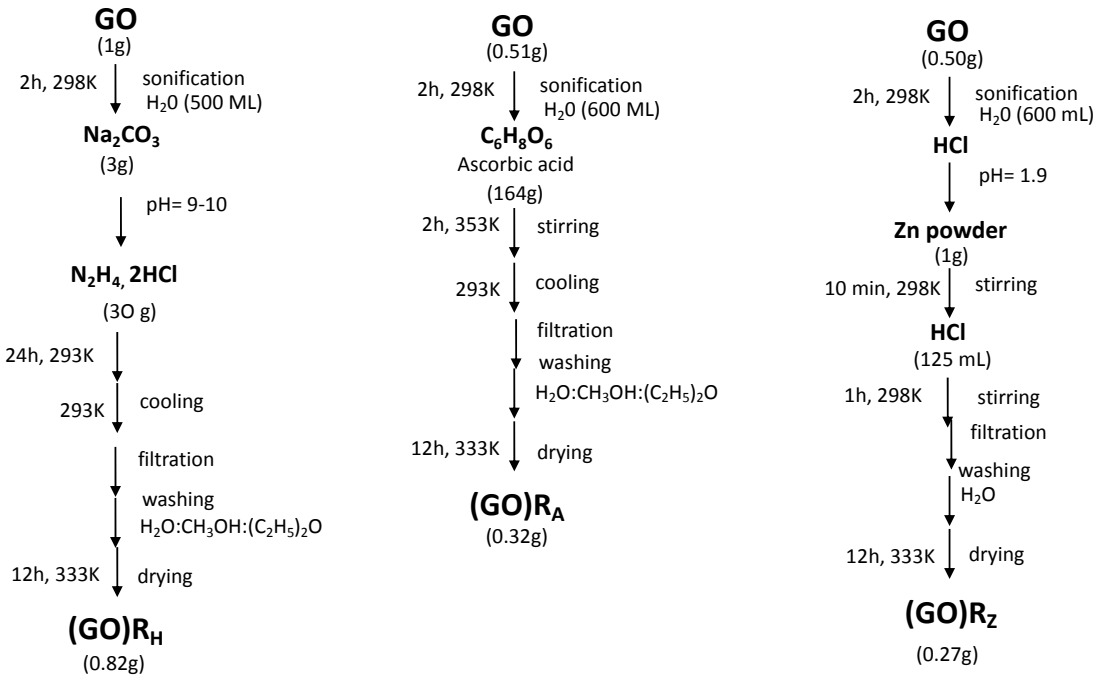

879

880 **Figure S2.** Diagram of synthesis of the reduced graphene oxide.

881

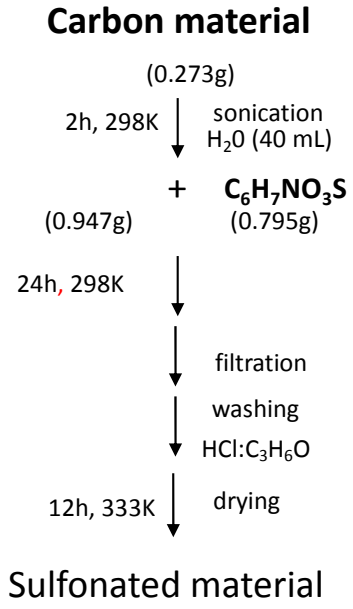

882

883 **Figure S3.** Diagram of synthesis of the sulfonated reduced graphene oxide.

884

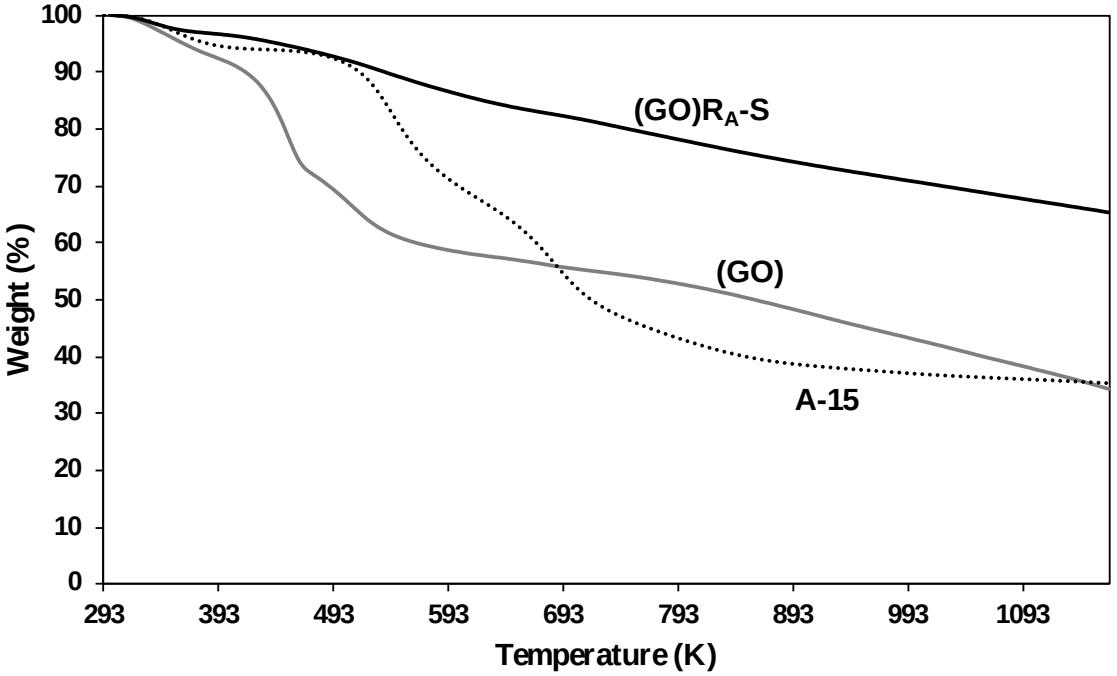

Figure S4. TGA pattern of (GO)R_A-S, (GO) and A-15.

Thermal stability study was carried out. **Figure S4** compares the TGA curves of Amberlyst® 15, (GO) and (GO)R_A-S. The overall weight loss of 64.5 % for GO occurs in three successive steps. The first one is a steady weight loss of 7.7 % attributed to the vaporization of adsorbed water molecules and occurs at around 393 K. Then a rapid loss of 20% due to the decomposition of the oxygen-containing functional groups such as hydroxyl, epoxy, carbonyl, and carboxyl groups in the temperature range of 393-473 K. Finally, a weight loss of 36.8 % that can be attributed to the combustion of the carbon skeleton is observed in the temperature range of 273–1163 K [1]. TGA curve for (GO)R_A-S show overall less than 35 % weight loss in the same temperature range. A first mass loss of 4.4 % at around 373 K was attributed to volatiles desorption, mainly moisture. A second weight loss of 11.8 % at around 648 K that can be attributed to the decomposition of

remnants oxygen groups (hydroxyl, epoxy, carbonyl, and carboxyl). The weight loss in the temperature range 648-1163 K can be attributed to decomposition of sulfonated groups [1]. The degradation of Amberlyst®15 proceeds in three steps: dehydration at 403 K, desulfonation at 508–603 K and oxidation of polymer at 603–828 K, representing a weight loss of 60.7 % at 873 K. These results suggest that the (GO)R_A-S is more thermally stable than the reference catalyst Amberlyst® 15, which allows its use in acid reactions at temperatures in which the A-15 can not be used.

[1] F. Liu, J. Sun, L. Zhu, X. Meng, C. Qi and F.-S. Xiao, *J. Mater. Chem.*, 2012, **22**, 5495-5502.